Injectable Sensors Based on Passive Rectification of Volume-Conducted Currents

Shahid Malik ⬤, Quim Castellví ⬤, Laura Becerra-Fajardo ⬤, Marc Tudela-Pi ⬤, Aracelys García-Moreno ⬤, Maryam Shojaei Baghini ⬤, and Antoni Ivorra ⬤

Abstract—Sensing implants that can be deployed by catheterization or by injection are preferable over implants requiring invasive surgery. However, present powering methods for active implants and present interrogation methods for passive implants require bulky parts within the implants that hinder the development of such minimally invasive devices. In this article, we propose a novel approach that potentially enables the development of passive sensing systems overcoming the limitations of previous implantable sensing systems in terms of miniaturization. In this approach implants are shaped as thread-like devices suitable for implantation by injection. Their basic structure consists of a thin elongated body with two electrodes at opposite ends and a simple and small circuit made up of a diode, a capacitor and a resistor. The interrogation method to obtain measurements from the implants consists in applying innocuous bursts of high frequency (≥ 1 MHz) alternating current that reach the implants by volume conduction and in capturing and processing the voltage signals that the implants produce after the bursts. As proof-of-concept, and for illustrating how to put in practice this novel approach, here we describe the development and characterization of a system for measuring the conductivity of tissues surrounding the implant. We also describe the implementation and the *in vitro* validation of a 0.95 mm-thick, flexible injectable implant made of off-the-shelf components. For conductivities ranging from about 0.2 to 0.8 S/m, when compared to a commercial conductivity meter, the accuracy of the implemented system was about $\pm 10\%$.

Index Terms—Biomedical transducers, implants, implantable sensor, galvanic coupling, volume conduction.

I. INTRODUCTION

IMPLANTABLE sensing systems are mainly motivated by the need to monitor clinically relevant magnitudes directly in the body regions where the physiologically relevant events take place [1].

Some implantable sensing systems are already used in clinical practice. For instance: glucose sensors for diabetic patients [2], pH sensors for monitoring gastroesophageal reflux [3] and blood pressure sensors for monitoring heart failure [4]. Remarkably, the number of commercially available systems is very small in contrast with the breath of academic research in the field of implantable sensors [1]. Market and regulatory issues are likely culprits of such discrepancy. However, other practical factors also explain this situation. Among those factors is invasiveness: systems that require highly invasive surgeries to implant the devices are unlikely to be adopted if less invasive, or non-invasive, solutions exist; even if those solutions are sub-optimal regarding their performance [5].

Existing implantable sensing systems can be classified into three categories according to the electronics the implants contain:

1) Implants with active electronics. The implants in this category contain a mechanism to generate electric energy which is used to power an electronic circuit capable of reading and processing the signal from a sensor and of transmitting the result to an external unit for further processing or representation. In some cases the electric power is entirely generated internally (e.g. with electrochemical batteries, [3]) and in other cases the electric power is either generated by transforming a sort of energy already present in the body (e.g. so-called energy harvesters can transform kinematic energy into electric energy, [6]) or by wireless power transmission from an external unit (e.g. ultrasound or inductive coupling power transmission, [2]). In all these cases, among other major drawbacks [7], the mechanism for generating the electric energy requires bulky parts that hinder miniaturization of the implants.

2) Implants with passive electronics. The implants in this category do not contain a mechanism to power the circuit. This is the category of the systems we propose here. To the best of our knowledge, with the exception of a recently proposed ultrasonic system [8], all the existing systems in this category are based on combinations of inductors and capacitors (LC systems) that resonate at a specific

frequency when an alternating magnetic field is applied. Such frequency is typically determined by a capacitor which acts as the sensor as its capacitance depends on the magnitude of interest [9]. An example of these systems is the CardioMEMS HF System by St. Jude Medical [4]. The main disadvantage of these systems is that they require coils with a relatively large diameter both at the implant and at the external unit. For instance, the implant of the CardioMEMS HF System contains a coil of about 3 mm × 8 mm.

3) Non-electronic implants. In the implants in this category the magnitude of interest is transduced into a non-electrical magnitude which is read and processed by a remote unit. To the best of our knowledge, the only systems available of this type are based on transduction into optic properties and, in particular, into fluorescence (e.g. Lumee systems by Profusa, Inc., [10]). The major drawback of these systems is that they are limited to applications in which the sensor is very close to the external unit so that optical transmission is feasible.

Here we propose a novel approach that may allow the development of passive sensing systems that overcome the limitations of previous implantable sensing systems in terms of miniaturization.

The implants according to this novel approach can be shaped as thread-like devices suitable for implantation by injection. Their basic structure consists of a thin elongated body with two electrodes at opposite ends and a simple and small circuit made up of a diode, a capacitor and a resistor.

The interrogation method to obtain measurements from the implants consists in applying innocuous bursts of high frequency (≥ 1 MHz) alternating current that reach the implants by volume conduction and in capturing and processing the voltage signals that the implants produce after cessation of each burst.

As proof-of-concept, and for illustrating how to put in practice this novel approach, here we describe the development and characterization of a system for measuring the conductivity of tissues surrounding the implant. The developed system can be portrayed as a system for measuring tissue electrical impedance, also known as electrical bioimpedance or simply as bioimpedance. Measurement and monitoring of bioimpedance offers interesting insights about the state of a tissue, which helps in monitoring and diagnosing different medical conditions [11].

II. METHODS

A. System Overview

The system schematically represented in Fig. 1 serves to disclose the proposed approach. The system consists of an implant and an external unit able to interrogate it.

The implant consists of a passive electronic circuit and two electrodes connected to that circuit. The implant is shaped as a thin elongated body with the two electrodes at opposite ends. The fundamental structure of the implant circuit consists of an element of asymmetric conductance (a diode, D_{im}, in Fig. 1) in series with a capacitor C_{im} and an element able to discharge the capacitor (resistor R_{im}).
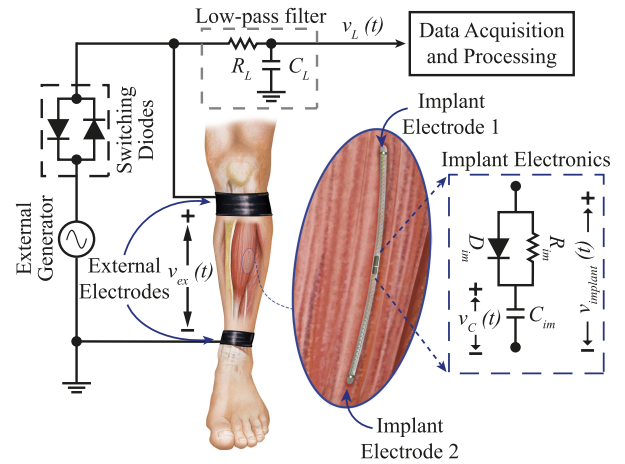

Fig. 1. Schematic representation of a hypothetical system according to proposed approach. Two external textile electrodes are strapped around the lower leg, where a passive implant with two electrodes has been intramuscularly deployed. The electronics of the implant consists of a diode, a capacitor and a resistor. The external electrodes are connected to a generator of high-voltage ac bursts. A set of switching diodes automatically disconnects the electrodes from the generator in between bursts. The voltage signals produced by the implant after the bursts are captured and postprocessed to obtain a measurement of interest. In the proof-of concept of this study, the system is used for measuring the conductivity of tissues surrounding the implant.

The external unit interrogates the implants by delivering bursts of high frequency (≥ 1 MHz) alternating current across a pair of surface electrodes. These current bursts reach the implants by volume conduction and, because of rectification by the implant diode, charge the implant capacitor. After burst cessation, the capacitor discharges through the discharging resistor and through the tissues across the implant electrodes. This creates a decaying voltage signal across the implant electrodes that, again thanks to volume conduction, can be sensed by the external unit across the pair of external electrodes. The time course of this signal depends on the characteristic values of the three electronic components of the implant circuit – any of which can act as a transducer for a magnitude of interest – and on the impedance seen by the implant circuit, which consists of the impedances of the implant electrodes, Z_e, and the impedance of the tissues across the implant electrodes, Z_{tissue}. For the application scenario considered here (i.e. conductivity sensing), the three components of the implant circuit are of fixed value and the time course of the signal is determined by the impedance seen by the implant circuit. If tissue impedance can be approximated by a resistance, R_{tissue}, and Z_e can be neglected, then the voltage across the implant electrodes, $v_{implant}$, will correspond to an exponential decay

$$v_{implant}(t) = Ae^{-t/\tau} \tag{1}$$

where A is the initial voltage that appears across the implant electrodes after the burst due to the accumulated charge in C_{im}. And the time constant, τ, is

$$\tau = C_{im}(R_{im} + R_{tissue}) \tag{2}$$

In a more general scenario, the measurand of interest (x) would be related to the value of any of the above parameters (y) through a transfer function ($y = g(x)$) and it would be possible to compute a measurement by applying the inverse function

$(x' = g^{-1}(y'))$ to the estimated value for the parameter (y'). For instance, if the capacitor of the implant acts as a pressure transducer, then x would be the pressure, y would be C_{im} and the function g would be the characteristic transfer function of such pressure transducer.

It must be noted that the capacitor of the implant serves a dual purpose. In addition to acting as a fundamental functional element of the sensing structure, it prevents the passage of dc currents through the implant electrodes that would cause electrochemical reactions and thus, damage both the electrodes and the tissues [12].

The external unit must include a switching mechanism to disconnect the external generator from the two external electrodes when the burst ends. This is needed to prevent short-circuiting the voltage signal from the implant. Otherwise, it would not be possible to detect the decaying voltage signal across the external electrodes. In the system represented in Fig. 1. the automatic switching mechanism consists of two antiparallel switching diodes. This mechanism allows passage of large voltage signals (the signal applied by the external generator during the burst) but blocks passage of small voltage signals (the voltage signal generated by the remote implant after burst cessation, that is, in between bursts).

The external unit also comprises a signal acquisition and processing sub-system. This sub-system is preceded by a simple low-pass filter which is intended to suppress noise and interferences and, more importantly, to prevent saturation or damage to the signal acquisition subsystem during burst delivery. The low-pass filter has a high enough cutoff frequency to prevent distorting the signal from the implant. As later explained, processing consists in characterizing the time course of the detected voltage signal. If the time course corresponds to an exponential decay, then the characterization can simply consist in finding the value of the time constant, τ.

Fig. 2 displays illustrative waveforms of the system. The implant capacitor charges during the delivery of the burst and discharges through the resistor and tissues after burst cessation. This discharge is detected as a small decaying voltage signal across the external electrodes. Its magnitude will be much smaller due to the attenuation through the volume conduction channel between the implant electrodes and the external electrodes. Additionally, as the tissues behave as a low-pass filter [13], the decaying voltage signal generated across the implant electrodes and detected at the external electrodes may be slightly distorted. However, as discussed below, we do not expect such distortion to be significant.

A key aspect of the proposed approach is that the injected alternating currents for interrogation, which can be either current controlled or voltage controlled, are innocuous. This is accomplished by ensuring that the supplied currents are of enough frequency to prevent unwanted stimulation of excitable tissues and by ensuring that their power is low enough to prevent excessive heating of tissues because of Joule heating. In a preceding study in which we propose the use of volume conduction to power active implants, we lengthy discuss the implications of these two restrictions on the permissible characteristics of the applied alternating currents [14]. Here we briefly overview these implications.
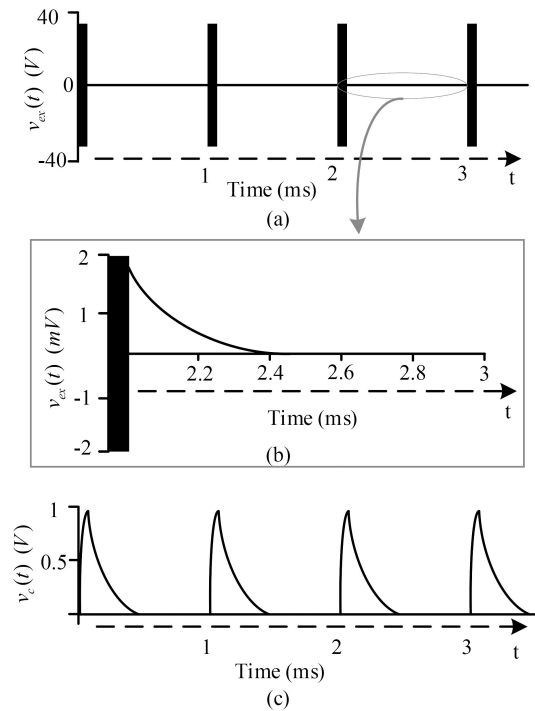

Fig. 2. Characteristic waveforms of the system. (a) Voltage across the external unit electrodes ($v_{ex}(t)$). (b) Magnification of voltage across the external electrodes. (c) Voltage across the implant capacitor ($v_C(t)$).

Unwanted stimulation of the excitable tissues can be avoided by using alternating currents above 100 kHz [15]. It must be noted, however, that alternating currents above 10 MHz may not be convenient as at those frequencies the skin effect may be very substantial [16] and the operation of implants located deep inside the body would be hindered. Because of equipment limitations at the execution of the present study, the frequency of the alternating currents experimentally assayed here was 1 MHz. Although such frequency is high enough to prevent unwanted stimulation, we do recommend the use of frequencies slightly above 5 MHz (but below 10 MHz) to meet the limitations imposed by safety standards referred below. This issue is further clarified in the discussion section.

As we have demonstrated previously [14], tissue heating can be avoided by supplying the alternating currents in the form of short bursts rather than continuously.

The safety standards developed by the IEEE [17] and the International Commission on Non-Ionizing Radiation Protection (ICNIRP) [18] limit heating by specifying a threshold for the so-called Specific Absorption Rate (*SAR*) which corresponds to the power absorbed per mass of tissue and can be calculated as

$$SAR = \frac{\sigma(E_{\text{rms}})^2}{\rho} \tag{3}$$

where E_{rms} is the root mean square of the electric field applied in the tissues (V/m), σ is the electrical conductivity of the tissue (S/m) and ρ is the mass density of the tissue (kg/m^3). If a sinusoidal field is applied in the form of bursts, for a given bursts

repetition frequency, F (Hz), and burst duration, B (s),

$$SAR = \frac{FB\sigma(E_{\text{peak}})^2}{2\rho} \tag{4}$$

where E_{peak} is the amplitude of the electric field (V/m).

Both the IEEE standard and the ICNIRP guidelines indicate the same *SAR* limitations averaged over 6 minutes for localized exposure in the frequency range from 100 kHz to 3 GHz. For general public and at any human body location, the *SAR* limit is 2 W/kg. If (4) is particularized for the case of muscle tissue at 1 MHz ($\sigma_{1\text{ MHz}} = 0.50$ S/m [19], $\rho = 1060$ kg/m^3 [20]) and assuming that $F = 1$ kHz, $B = 100$ μs, the maximum admissible field amplitude would be 290 V/m. The field amplitude used in the experiments reported here was 200 V/m which in muscle would produce a *SAR* of 0.94 W/kg, which is below the maximum safety threshold.

A stringent requirement for the conformation of the implants is that the separation distance between its two electrodes, l, must be large enough so as to pick up a voltage difference sufficient for the operation of the circuit. That is, the separation distance must be larger than the minimum voltage for operation divided by the expected electric field magnitude (E_{peak}) at the location of the implant. The diode will require a minimum voltage in the order of hundreds of millivolts for operation. Because of the safety considerations described above and taking into account that the maximum allowable electric field amplitude at the location of the implant will be in the order of a very few volts per centimeter, the diode voltage requirement translates in a minimum inter electrode distance in the order of a few millimeters. However, considering that the implant may not be perfectly aligned with the electric field and other uncertainties, we deem that in most application scenarios the separation distance will have to be in the order of a centimeter or a very few centimeters. In the experiments reported here the separation distance (l) was 25 mm which for a field magnitude of 200 V/m corresponds to a maximum (open circuit) voltage across implant electrodes of 5.0 V.

B. Modeling of the System

As in previous cases in which volume conduction has been proposed to communicate with or to transfer power to electronic implants [21]–[23], the system studied here can be modeled with the assistance of a two-port reciprocal network for representing coupling between the external unit circuitry and the implant circuit (Fig. 3 and Fig. 4). The two-port network accounts for the impedances of the external electrodes, the impedances of the implant electrodes and the impedances that couple the external electrodes to the implant electrodes. Voltages and currents at the network are expressed as

$$\begin{bmatrix} V_1 \\ V_2 \end{bmatrix} = \begin{bmatrix} Z_{11} & Z_{12} \\ Z_{12} & Z_{22} \end{bmatrix} \begin{bmatrix} I_1 \\ I_2 \end{bmatrix} \tag{5}$$

where V_1 is the voltage across the two external electrodes (i.e., v_{ex}) and V_2 is the voltage across the implant electrodes (i.e., $v_{implant}$), I_1 is the current through the two external electrodes and I_2 is the current through the implant [22].
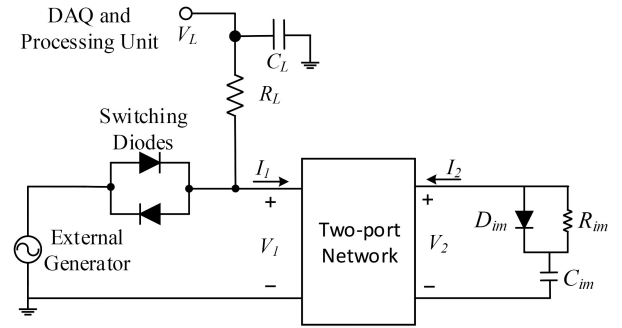

Fig. 3.   Coupling between the terminals of the external system and the terminals of the implant can be modeled with a two-port network. $\boldsymbol{V}_1$ is the voltage across the two terminals of the external system (i.e., $\boldsymbol{v_{ex}(t)}$) and $\boldsymbol{V}_2$ is the voltage across the two terminals of the implant electronics (i.e., $\boldsymbol{v_{implant}(t)}$).
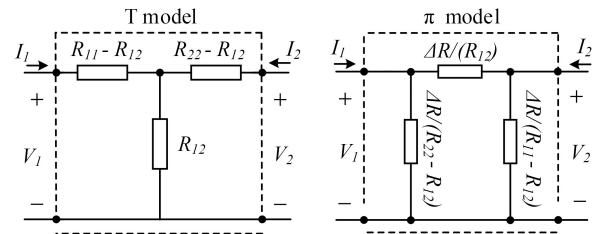
Fig. 4.   T and π models for the two-port network. ($\boldsymbol{\Delta R} = \boldsymbol{R_{11}R_{12} - R_{12}^2}$).

For the sake of simplicity, the impedances in the two-port network can be substituted by resistances so that

$$\begin{bmatrix} V_1 \\ V_2 \end{bmatrix} = \begin{bmatrix} R_{11} & R_{12} \\ R_{12} & R_{22} \end{bmatrix} \begin{bmatrix} I_1 \\ I_2 \end{bmatrix} \tag{6}$$

This simplification is reasonable if the impedance of the electrodes is low in comparison to the impedances of the other elements of the system and if tissue impedances can be approximated as resistances. As it will be shown later, this simplification produces accurate results in the *in vitro* scenarios considered here.

By definition

$$R_{11} \overset{\text{def}}{=} \frac{V_1}{I_1}\bigg|_{I_2=0}, R_{22} \overset{\text{def}}{=} \frac{V_2}{I_2}\bigg|_{I_1=0}, R_{12} \overset{\text{def}}{=} \frac{V_1}{I_2}\bigg|_{I_1=0} \tag{7}$$

Therefore, R_{11}, R_{22}, and R_{12} can be obtained by imposing the conditions expressed in (7). This can be done experimentally (i.e. applying signals and performing measurements), by means of numerical modeling and, in some simple cases, by means of analytical expressions [22]. For instance, for R_{22} (i.e. resistance across implant electrodes), if the implant electrodes are approximated as spheres at a separation distance, l, much larger than their diameter, D, then the following known analytical expression can be applied

$$R_{22} = \frac{1}{\sigma\pi D} \tag{8}$$

where σ is the conductivity of the medium [24].

As explained in [22], once the network model for the coupling between the external electrodes and the implant electrodes is obtained, the behavior of any circuit topology–including those that are non-linear–for the implant or for the external system can

be easily studied with the help of circuit simulators. For that, the T or π models of the two-port network can be employed. (Fig. 4).

C. Signal Processing

The voltage signal picked-up by the external electrodes ($v_L(t)$) after the burst ends is proportional to the voltage across the implant electrodes ($v_{implant}(t)$) but is very feeble and is buried in noise. To extract the parameter of interest, y, from such feeble signal we propose a signal processing scheme that can be divided in two stages: 1) to band-pass filter the signal and to average multiple acquisitions corresponding to multiple bursts and 2) to fit the average recorded signal ($\bar{v}_L(t)$) to a model corresponding to the expected pattern for the implant voltage ($v_{implant}(t)$) by adjusting the estimation, y', of the parameter of interest. Fitting can be performed using known curve fitting procedures such as those based on the least squares method [25]. In the application scenario considered here (i.e. measurement of tissue conductivity, σ) and assuming the approximations indicated above (i.e. $Z_e = 0$; $Z_{tissue} = R_{tissue}$), we can fit this model as (1). Since we model R_{tissue} as R_{22} from (8), (2) becomes

$$\tau = C_{im}\left(R_{im} + \frac{1}{\sigma\pi D}\right) \qquad (9)$$

As the time constant τ is proportional to the values of C_{im} and R_{im}, the values of these components should be defined such that the capacitor practically fully discharges after the burst (i.e. $\tau \ll 1/F$). However, these values cannot be too low. For sensitivity and repeatability, C_{im} must be higher than the parasitic capacitance across the implant, which can have values in the order of tens of picofarads. Additionally, R_{im} cannot be too small to prevent short-circuiting the device. For the conditions assayed here ($F = 1$ kHz, $D = 0.5$ mm and $\sigma > 0.1$ S/m), R_{im} values in the order of a few kilohms and C_{im} values in the order of a very few tens of nanofarads meet these requirements.

From (9), the estimated conductivity is.

$$\sigma' = \frac{1}{\left(\frac{\tau}{C_{im}} - R_{im}\right)\pi D} \qquad (10)$$

D. First Experimental Setup: Pair of Electrodes in a Bath of Saline Solution

The first experimental setup is represented in Fig. 5. In it, the living tissues were modeled by a bath of saline solution and the implant was modeled by two spherical electrodes connected with wires to an external passive circuit with the structure described above. Diode, D_{im}, was a Schottky diode (1N5817 by Diodes Incorporated), the capacitor, C_{im}, had a capacitance of 14.7 nF, and the resistor, R_{im}, had a resistance of 2.3 kΩ (values measured with a commercial multimeter (38XR-A by Amprobe)).

The saline bath consisted of a rectangular plastic container filled with a NaCl solution. (Different NaCl concentrations were assayed.) At the inner opposite ends of the container, aluminum plates were glued acting as the external electrodes. The dimensions of the bath were 84 mm $\times$ 150 mm $\times$ 30 mm.

The implant electrodes consisted of two stainless steel spheres with a diameter, D, of 0.5 mm at a separation distance, l, of
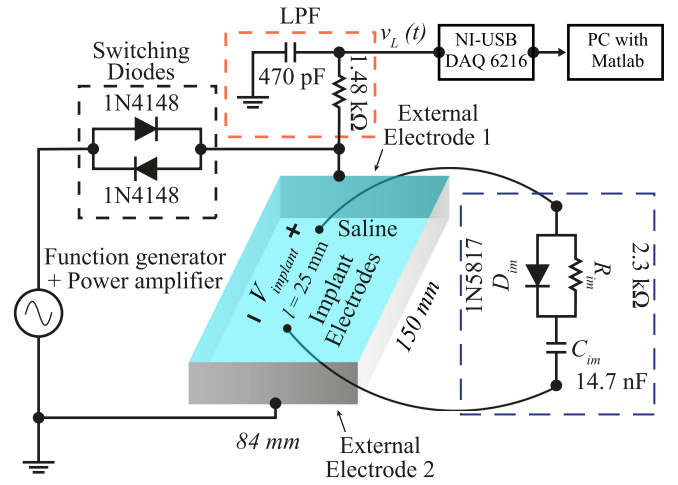

Fig. 5. *In vitro* setup for illustrating the behavior of the proposed sensing approach when set for measuring medium conductivity. The living tissues are modeled by a bath of saline solution and the implant is modeled by two spherical electrodes connected with insulated wires to an external passive circuit with the implant electronics.

TABLE I
EXPERIMENTAL SETUP FOR THE SALINE MEDIUM

Parameters	Values
Applied electric field	
E_{peak}	200 V/m
Frequency, f	1 MHz
Burst frequency, F	1 kHz
Burst duration, B	100 μs
Saline medium	
Dimensions	$84 \times 150 \times 30$ mm^3
Conductivity σ (S/m)	0.22, 0.32, 0.42, 0.50, 0.63, 0.78
Implant electrodes	
Diameter, D	0.5 mm
Material	Stainless steel
Separation distance, l	25 mm
Implant circuitry	
Capacitor, C_{im}	14.7 nF
Resistor, R_{im}	2.3 kΩ
Diode, D_{im}	1N5817

25 mm. Each electrode was laser welded to a 45 cm piece of 32 AWG enameled copper wire for connection with external circuits. A cotton thread running from a hole at the center of one plate electrode to another hole at the center of the other plate electrode tied the electrodes and held them at the center of the bath. The details of the experimental setup are tabulated in Table I.

The interrogation system is also depicted in Fig. 5. An external generator composed of a function generator (BK4064 by BK Precision) followed by a high voltage amplifier (WMA 300 by Falco Systems), was used to generate the interrogation signal. This signal consisted in sinusoidal bursts with a frequency f of 1 MHz, a duration B of 100 μs, a repetition frequency F of 1 kHz

and an amplitude of 30 V. The signal was applied to the external electrodes through the switching system described above which in this case consisted of two 1N4148 diodes. A low-pass filter was also connected across the external electrodes. The output V_L of the low-pass filter was acquired by a data acquisition (DAQ) board (NI-USB6216 by National Instruments Corp.) with a resolution of 16 bits and sampling rate of 400 kS/s. The full scale of the ADC was programed at ±10 V which implies an absolute accuracy of 2.71 mV according to its specifications [26]. Signal acquisition in MATLAB (R2018a) was triggered by the signal generator at the end of each burst. Each acquisition (i.e. recording of filtered V_L after of the burst) was stored in MATLAB, 100 acquisitions of the signal were averaged and then fitted to a time exponential decay with the MATLAB curve fitting tool.

According to (10), and the values defined for F, C_{im}, R_{im} and D, the minimum conductivity that could be measured with this setup would be 0.06 S/m to ensure that the capacitor fully discharges in between bursts ($5\tau < (1/F - B)$).

To validate the assumptions regarding the behavior of the entire system, the setup was modeled in a two-step process. First, the π-model of the two-port network that represents coupling between the external electrodes and the implant electrodes was obtained by simulating the setup in a numerical software platform based on the finite element method (COMSOL Multiphysics 4.4). More specifically, in COMSOL the geometry of the bath and the electrodes, as represented in Fig. 5, was modeled. The so-called physics "Electric Currents (ec)" was used to obtain the dc parameters R_{11}, R_{22}, and R_{12} for different conductivities of the bath. These parameters were extracted by simulating the injection of unitary currents through the external electrodes or the implant electrodes and by measuring the resulting voltage differences (as indicated in (7)). For instance, the value R_{11} was obtained by simulating the injection of a current of 1 A between the external electrodes and measuring the voltage across them. The mesh used by the solver consisted of 230245 tetrahedral elements. Once the R parameters were obtained, the values of the π-model were calculated as indicated in Fig. 4. In the second step of the modelling process, the complete setup was simulated in a circuit simulator (NI-Multisim 14.1) by incorporating the obtained π-model in the circuit model represented in Fig. 3. The voltage $v_L(t)$ was obtained as direct result of the circuit simulator.

The true conductivity of the saline solution was estimated using two different measurement methods. The first method consisted in applying across the implant electrodes a sinusoidal signal with known amplitude and measuring the current using a current probe (TCP2020 by Tektronix, Inc). A digital oscilloscope (TPS2014 by Tektronix, Inc) was used to measure the amplitude of the excitation voltage and current. The resultant impedance values were used with (7) to measure the conductance of the saline solution. The second method to obtain the reference conductivity of the saline solution consisted in using a calibrated commercial conductance meter (H198312 DIST 6 by Hanna Instruments).

The same setup was also used to validate the behavior of the system when the implant is oriented at different angles with respect to the external electrodes. The maximum voltage attainable at the implant depends on the angle of the implant with respect to the field applied by the external electrodes [21]. Assuming a homogeneous medium with a uniform electric field, the maximum voltage across the implant electrodes will be

$$V_{implant_{peak}} = \overrightarrow{E_{peak}} \cdot \vec{l}$$
$$= E_{peak}\, l\, \cos\theta \qquad (11)$$

where $\vec{l}$ is the vector defined by the position of the two implant electrodes and θ is the angle formed by this vector and the electric field. If the implant is aligned with the electric field, as it is the case represented in Fig. 5, the voltage across the implant electrodes is maximized. For other angles, the maximum voltage attainable at the implant is proportionally lower and hence it is also lower the magnitude of the discharge signal it produces after burst cessation. Furthermore, since the discharge field produced by the implant is not aligned with the external electrodes, the magnitude of the detected signal across the external electrodes is further lowered. Therefore, misalignments will significantly worsen the signal-to-noise ratio. However, if the parameter of interest is not related to the amplitude of the signal, as it is the case here (τ), misalignments will not distort the measurements. Here, this was experimentally verified for misalignment angles of up to 45 °.

E. Second Experimental Setup: Proof-of-Concept Implant Injected Into Agar Phantom

A proof-of-concept implant was built with commercial off-the-shelf components. It consisted of a short silicone tubing (diameter 0.95 mm, length 24 mm) that housed a flexible PCB (0.7 mm $\times$ 5 mm) connected with two pieces of 32 AWG enameled copper wire to two stainless steel spheres with a diameter of 0.5 mm located at the opposite ends of the tubing. The silicone tube is custom-made by Freudenberg Medical Europe GmbH manufactured from medical grade silicone elastomer (MED-4050 by NuSil Technology) with an outer diameter of 0.92 mm and wall thickness of 100 μm. The tube was filled with a low viscosity medical grade silicone elastomer (MED-6015 by NuSil Technology). This expands the tube to a final outer diameter of approximately 0.95 mm. The implant circuit represented in Fig. 1 was mounted on the PCB, where the diode, D_{im}, was a schottky diode (RB521ZS-30 by ROHM Semiconductor), the capacitor, C_{im}, had a nominal capacitance of 10 nF (TMK063BJ103KP-F by Taiyo Yuden) and the resistor, R_{im}, had a nominal resistance of 2 kΩ (ERJ1GNJ102C by Panasonic). These values differ slightly from those used in the first experimental setup because of the need to use available miniature components that could fit inside the implant. According to (10), and the values defined in this experimental setup for F, C_{im}, R_{im} and D, the minimum conductivity that could be measured with this setup would be 0.04 S/m. The details of the experimental setup for the agar phantom are tabulated in Table II.

Four agar gel phantoms (84 mm $\times$ 150 mm $\times$ 24 mm rectangular prisms) of different conductivity were prepared to validate the operation of the implant. The first step in the preparation of

TABLE II
EXPERIMENTAL SETUP FOR THE AGAR PHANTOM

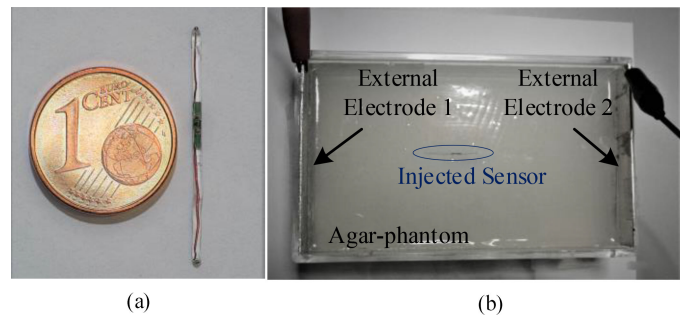| Parameters		Values
Applied electric field		
	E_{peak}	200 V/m
	Frequency, f	1 MHz
	Burst frequency, F	1 kHz
	Burst duration, B	100 μs
Saline medium		
	Dimensions	$84 \times 150 \times 24$ mm^3
	Conductivity σ (S/m)	0.26, 0.48, 0.58, 0.71
Implant electrodes		
	Diameter, D	0.5 mm
	Material	Stainless steel
	Separation distance, l	24 mm
Implant circuitry		
	Capacitor, C_{im}	10 nF
	Resistor, R_{im}	2 kΩ
	Diode, D_{im}	Schottky diode RB521ZS-30

(a)   (b)

Fig. 6. (a) Implemented proof-of-concept implant, and (b) The agar-phantom, external electrodes and the implant used in the *in vitro* setup used to validate the operation of the proposed approach. The implant was injected into a saline (NaCl) agar rectangular prism of specific conductivity and the interrogation signal was applied through aluminum plate electrodes acting as the external electrodes.
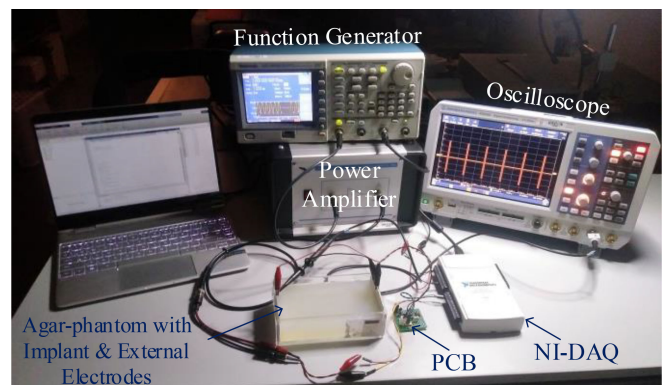

Fig. 7. *In vitro* measurement setup for illustrating the behavior of the proposed sensing approach. The implant was injected into the agar phantom. The external elements are those schematically represented in Fig. 5 plus the oscilloscope for monitoring the voltage from the power amplifier. The external PCB contains the low-pass filter and the switching diodes of Fig. 5.

the agar phantoms was the preparation of the agar base which simply consisted of a saline (NaCl) solution. (The conductivity of the agar gel is linearly related to the NaCl concentration and hence it can be set by adjusting the amount of NaCl salt diluted in distilled water [28].) The NaCl solution was then mixed with agar powder (A7002-500G from Sigma-Aldrich) at a concentration of 1.5 grams of agar powder per 100 ml of solution. Then, the conductivity of the mixture was measured at room temperature (20 °C) with the commercial conductivity meter (H198312 DIST 6 by Hanna Instruments). (The measured conductivities for the four prepared mixtures were found to be 0.26 S/m, 0.48 S/m, 0.58 S/m, and 0.71 S/m.) Finally, the mixture was heated until boiling, poured into a plastic mold and cooled down at room temperature until it jellified.

The implant prototype was injected into the jellified agar phantom using a 14G catheter (model 382268 by Becton, Dickinson and Company, NJ, USA) following the envisioned clinical implantation procedure. Such implantation procedure is described in the discussion and illustrated in Fig. 12.

After implantation, the agar phantom was then placed in a rectangular plastic box with two aluminum plate electrodes at opposite sides. As in the previous setup, these plate electrodes acted as the external electrodes. The same interrogation system described previously was used in this setup (Fig. 7).

III. RESULTS

A. Results From the Saline Bath Setup

For the setup of Fig. 5, Fig. 8 shows a sample acquisition of $v_L(t)$ after burst cessation together with the average of 100 acquisitions, $\bar{v}_L(t)$, and the result of fitting that average to an exponential decay, $\hat{v}_L(t)$. This example corresponds to the case of $\sigma = 0.22$ S/m (as measured by the conductivity meter) which, according to nominal values for D_{im}, R_{im} and C_{im} and to (9), produces a time constant (τ) of 76.3 μs which is close to the result of the fitting, 71.4 μs. Individual acquisitions were considerably noisy. This was probably due to capacitively and

magnetically coupled interferences as no specific precautions were taken in this regard (e.g. no shielding). Another possible cause is electrochemical noise at the plate electrodes [29], [30]. By averaging multiple acquisitions, this noise was significantly reduced, as shown in Fig. 8.

In Fig. 8, the amplitude of the detected signal, $v_L(t)$, was about 5 mV. This corresponds to a maximum voltage across the implant capacitor of about 600 mV and a maximum voltage across the implant electrodes of about 300 mV. Hence, the implant signal was attenuated approximately 36 dB.

Fig. 9 combines the experimental fittings ($\hat{v}_L(t)$), from all the assayed NaCl solutions, together with the simulated signal acquisitions ($v_L(t)$) obtained by modelling the entire setup with the circuit simulator after obtaining the two-port network models with COMSOL. Agreement between the experimental and the simulated time courses of the signals validates the stated assumptions.

Table III shows the measurement results together with the relative errors. The conductivity values were estimated with (10) using the estimations of the time constants (τ') provided by the fittings. The maximum relative error is less than $\pm 9.1\%$.
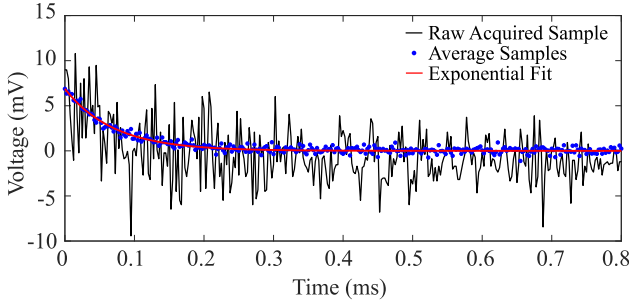
Fig. 8. For the setup of Fig. 5, experimental signals acquired by the DAQ board across the capacitor of the low-pass filter ($v_L(t)$) after burst cessation when the conductivity of the solution was 0.22 S/m. The discharge in the implant capacitor C_{im} produces a small decaying voltage signal across the external electrodes. It is displayed a sample acquisition of $v_L(t)$ together with the average of 100 acquisitions, $\bar{v}_L(t)$, and the result of the fitting to an exponential decay, $\hat{v}_L(t)$. The implant electrodes were perpendicular to the external electrodes, $\theta = 0$.
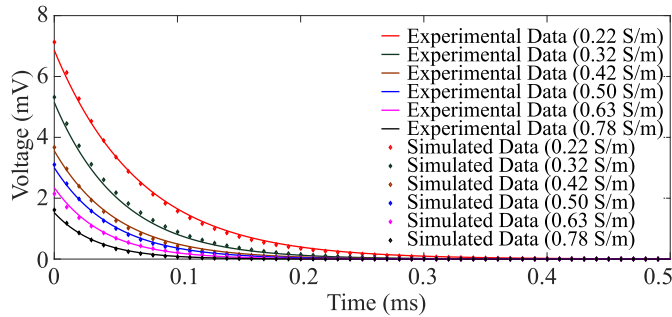

Fig. 9. For the setup of Fig. 5, experimental exponential fittings ($\hat{v}_L(t)$) from all the assayed NaCl solutions together with the simulated signal acquisitions ($v_L(t)$) obtained by modeling the entire setup with the circuit simulator. (The implant electrodes were perpendicular to the external electrodes, $\theta = 0$.) The exponential fittings ($\hat{v}_L(t)$) were computed after averaging 100 acquisitions.

TABLE III
EXPERIMENTAL RESULTS WITH THE SALINE MEDIUM

Conductivity measurement with commercial meter (S/m)	Measurements with the setup of Fig. 5 (S/m)	Relative error (%)
0.22	0.20	-9.1
0.32	0.33	3.2
0.42	0.44	4.8
0.50	0.52	4.0
0.63	0.62	-1.6
0.78	0.77	-1.3

For a saline conductivity of 0.51 S/m, Fig. 10 shows for different alignment angles the experimental fittings ($\hat{v}_L(t)$) together with the simulated signal acquisitions ($v_L(t)$). As expected, the amplitude of the signal for $\theta = 45°$ is much lower than that for $\theta = 0°$. However, this does not have a direct impact on the estimated time constant ($\tau'_{0°} = 67.0\,\mu s$, $\tau'_{45°} = 67.4\,\mu s$) and, hence, does not have an impact on the conductivity measurements ($\theta'_{0°} = 0.51$ S/m, $\theta'_{45°} = 0.50$ S/m).
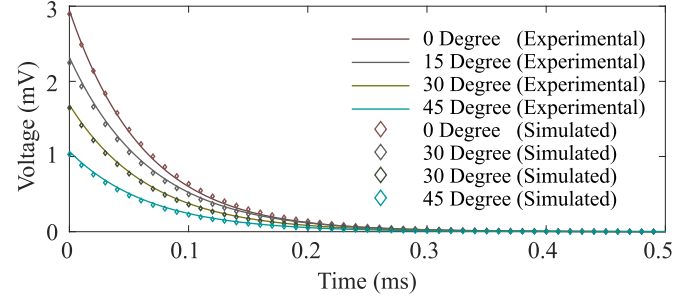

Fig. 10. For different alignment angles, experimental exponential fittings ($\hat{v}_L(t)$) together with the simulated signal acquisitions ($v_L(t)$) obtained by modeling the entire setup with the circuit simulator. The solution conductivity was 0.51 S/m. The exponential fittings ($\hat{v}_L(t)$) were computed after averaging 100 acquisitions.
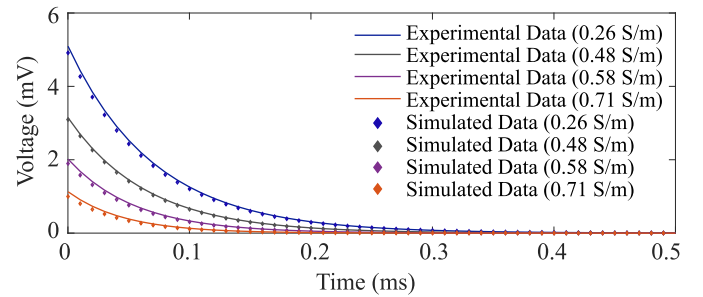

Fig. 11. For the proof-of-concept implant and the setup of Fig. 6, experimental exponential fittings ($\hat{v}_L(t)$) from the four assayed phantoms together with the simulated signal acquisitions ($v_L(t)$) obtained by modeling the entire setup with the circuit simulator. The exponential fittings ($\hat{v}_L(t)$) were computed after averaging 100 acquisitions.

TABLE IV
EXPERIMENTAL RESULTS WITH THE PROOF-OF-CONCEPT IMPLANT

Conductivity measurement with commercial meter (S/m)	Measurements with the proof-of-concept implant (S/m)	Relative error (%)
0.26	0.25	-3.9
0.48	0.46	-4.2
0.58	0.56	-3.5
0.71	0.74	4.3

B. Results With the Proof-of-Concept Implant Injected Into Agar Phantom

The conductivity of the agar phantom was measured using the proposed approach. Four agar phantoms of different conductivity were prepared.

Table IV shows the measurement results together with the relative errors. The conductivity values were estimated with (10) using the estimations of the time constants (τ') provided by the fittings. The maximum relative error in this case was less than $\pm 4.3\%$.

IV. DISCUSSION

The application scenario developed here (i.e. conductivity measurement) was merely intended to demonstrate the proposed

sensing approach and to illustrate how to put it in practice. However, it is worth noting that it may have some real medical applications. For instance, it could be used to measure the conductivity of the lungs for monitoring congestive heart failure. Pulmonary edema, that is, accumulation of fluids in the lungs, occurs during worsening heart failure [31]. Since such accumulation of fluids causes an increase in the conductivity of the lungs, the measurements provided by the implants could be used to determine when heart failure is worsening. Existing implantable pacemakers and defibrillators incorporate a similar functionality: they provide measurements of the so-called transthoracic impedance for early detection of worsening heart failure [32]. Those measurements are obtained by performing impedance measurements across the electrodes they possess for their therapeutic function. However, since these electrodes are implanted within large blood cavities (i.e. the heart ventricles and auriculas) and the conductivity of the blood is much higher than that of lung tissues, the measurements these systems perform exhibit low sensitivity to the conductivity of the lungs and, consequently, they exhibit reliability issues [33]–[35]. Furthermore, it must be noticed that only a minority of patients with congestive heart failure are implanted with a defibrillator or a pacemaker.

The proposed sensing approach is not limited to tissue conductivity or impedance measurements. Any measurand of interest with the potential to be transduced by any of the components of the implant could be measured with the proposed sensing approach. This, for instance, could be the case of pressure sensing via a capacitive pressure sensor for C_{im} or the case of temperature sensing via a thermistor for R_{im}. Less obvious cases could consist, for instance, in indirect transduction through optic properties. For example, the discharge could occur across a light sensitive conductive device (e.g. a photodiode) illuminated by a phosphorescent transducer material previously illuminated during the charging phase by a light-emitting diode.

In the above cases it would be necessary to avoid the impact of tissue impedance on the measurements. This can be achieved by, instead of using a resistor, implementing a discharge network that regulates the discharge current and hence making the discharge process independent of the impedance of the tissue. Such network can simply consist in a n-channel JFET with the gate shorted to the source [36].

Although in this study we have not attempted to characterize the measurement accuracy of the proposed approach, it is worth noting that the experimentally observed errors were very low. The results reported in Table III suggest that the systematic error was much lower than the random errors. It is not possible to provide a valid estimation of the systematic error with the limited amount of measurements reported in Table I but it is reasonable to guess that the magnitude of such systematic error was less than 0.01 S/m (5% for the smallest measurement) which probably is exceptionally low for a non-calibrated conductivity measurement system. Even taking into account that the characteristic values of the components of the implant and the dimensions were carefully measured, this value strikes us as very low. We presume we obtained such low systematic error by mere coincidence. On the other hand, in Table III it is also hinted that random errors (i.e. due to noise) are in the order of

about $\pm 5\%$. Although it is not reported here, we have observed that, as expected, the magnitude of these random errors largely depends on the number of averaged acquisitions. This implies an obvious tradeoff between accuracy and measurement speed.

The distance between external electrodes assayed in the experimental setups was 15 cm. Depending on the application in which the proposed sensing approach would be used, this distance could be considered excessive. We deem that in some applications the external system could consist in a small pod adhered to the skin, such as those used for implantable continuous glucose monitors [2]. The external electrodes could then be about 5 cm apart, thus allowing lower voltages for the interrogation signals or shorter implants.

For the sake of simplicity, in this study the impedances of the body tissues were approximated to resistances. This does not allow modeling the frequency dependent coupling between the external electrodes and the implant electrodes that will occur *in vivo*. Due to the impedance characteristics of living tissues [11], we anticipate that such coupling will coarsely behave as the combination of a voltage divider and a first order low-pass filter with a cutoff frequency in the order of a few tens of kilohertz. Consequently, we also anticipate that the shape of the signals generated across the implant electrodes (exponential decay with time constant in the order of 0.1 ms) will not be significantly distorted when it reaches the external electrodes. That is, we do not expect a significant impact on the time constant measurement due to the frequency dependent coupling that will appear in real scenarios. Nevertheless, this is an issue that must be addressed in detail in subsequent studies and *in vivo* validated.

Another limitation of this study was the use of a high voltage amplifier that in practice limited the frequency of the interrogation signal to 1 MHz. This frequency is high enough to prevent unwanted stimulation. However, we do recommend the use of frequencies slightly above 5 MHz (but below 10 MHz) to meet the limitations imposed by safety standards. For the field amplitudes assayed here, the applied 1 MHz bursts would not meet the IEEE safety standard [17] because of modulation harmonics. We discuss this issue in detail in [14]. Following the same procedure that is described in [14], if the waveform used here is applied to extremities ($f = 1$ MHz, $F = 1$ kHz, $B = 100$ μs), the permissible field magnitude would be about 160 V/m, below the magnitude assayed here (200 V/m). On the other hand, if the frequency (f) is increased to 5 MHz or to 6 MHz the permissible field increases to 840 V/m and 1400 V/m respectively.

Since a crucial feature of the proposed implants is that they can be implanted through an injection-like procedure, it is worth discussing about such implantation procedure. The procedure we envision for clinical implantation – which is the same we have used to deploy the proof-of-concept implant into the agar phantom – is represented in Fig. 12. The procedure is based on the use of clinical catheters. These catheters typically consist of two pieces: an outer flexible tube (i.e. the catheter *per se*) and an inner rigid tubular needle made of stainless steel (i.e. the needle used to introduce the catheter). In the proposed procedure, the catheter is introduced into the tissue as it is regularly done (steps a and b in Fig. 12). That is, the needle is used to pierce through the tissues and it is pulled out leaving the catheter in place. Then,
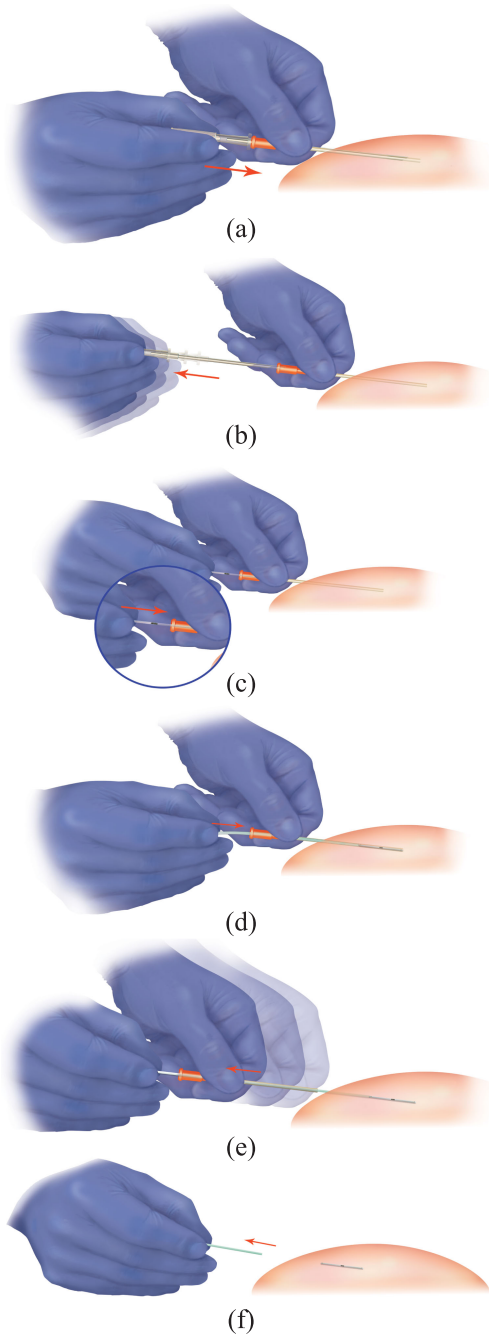
Fig. 12. Envisioned implantation procedure. (a) Catheter is inserted into the tissue of interest. (b) Needle of the catheter is extracted. (c) Implant is inserted in the catheter and (d) is pushed towards the end of the catheter. (e) Carefully, holding the pusher still, the catheter is removed, releasing the implant inside the tissue, and (f) the pusher is removed.

in the proposed procedure, the implant is introduced through the catheter and it is pushed inside to the distal point of the catheter with the help of a flexible cable (steps c and d). To finalize the procedure, the implant is deployed in place by pulling out the catheter while holding the flexible cable (step e) and afterwards the flexible cable is pulled out (step f).

We envision scenarios in which the implants would operate permanently and scenarios in which the implants would be left permanently implanted after their operational life. The passive characteristics of the implant electronics and the use of bio-compatible materials (e.g. silicone, titanium and noble metals for the packaging and the electrodes) would warrant permanent implantation as a safe option. However, it cannot be ruled out the necessity of extracting the implant due to infection, trauma or other potentially harmful circumstances. In these circum-stances, the implants would be removed through conventional surgical procedures if they had been implanted for a period long enough to cause adhesion to tissues. On the other hand, for short implantations, for instance for clinical trials, we envision the possibility of including an eyelet in one of the electrodes to facilitate extraction, as it has been assayed in previous wireless injectable devices [37], [38].

One concern regarding miniature wireless implants is the possibility of migration. We anticipate this will largely depend on the tissue where the implant is deployed. For cylindrical implants deployed intramuscularly, it has been shown that they do not migrate significantly over a year after their implantation [38]. However, if the implants are to be deployed in a location where mechanical stresses or flow of body fluids can cause their migration (e.g. inside an artery), fixation mechanisms will be required to prevent device failure and potential harmful conse-quences (e.g. embolization). For instance, anchoring tines, such as those used in commercial leadless pacing systems [39], could be added.

Finally, it must be noted that we have conceived the presented sensing approach after our work on injectable stimulators based on volume conduction and rectification [40]–[42]. In this regard, it is particularly relevant the study presented in [42] in which we *in vivo* demonstrated implants capable of neuromuscular stimulation whose structure is very similar to the structure of the proof-of-concept implant presented here.

V. CONCLUSION

In this paper, a novel approach is detailed that would allow the development of implantable passive sensing systems that may overcome the limitations of previous implantable sensing systems in terms of minimal invasiveness. In particular, it has been demonstrated that implants according to this novel ap-proach can be shaped as thread-like devices with a diameter below 1 mm, which are suitable for implantation by injection. As proof-of-concept, and for illustrating how to put in practice this novel approach, here it was described the development and characterization of a system for measuring the conductivity of tissues surrounding the implant. However, it is also hinted how this approach could also be applied for sensing other parameters such as pressure or temperature hence indicating the breadth of potential clinical applications for this novel approach.

ACKNOWLEDGMENT

REFERENCES

[1] A. Kiourti and K. S. Nikita, "A review of in-body biotelemetry devices: Implantables, ingestibles, and injectables," *IEEE Trans. Biomed. Eng.*, vol. 64, no. 7, pp. 1422–1430, Jul. 2017.

[2] M. P. Christiansen *et al.*, "A prospective multicenter evaluation of the accuracy of a novel implanted continuous glucose sensor: PRECISE II," *Diabetes Technol. Therapeutics*, vol. 20, no. 3, pp. 197–206, 2018.

[3] J. E. Pandolfino, J. E. Richter, T. Ours, J. M. Guardino, J. Chapman, and P. J. Kahrilas, "Ambulatory esophageal pH monitoring using a wireless system," *Amer. J. Gastroenterol.*, vol. 98, no. 4, pp. 740–749, 2003.

[4] J. T. Heywood *et al.*, "Impact of practice-based management of pulmonary artery pressures in 2000 patients implanted with the CardioMEMS sensor," *Circulation*, vol. 135, no. 16, pp. 1509–1517, 2017.

[5] R. D. Black, "Recent advances in translational work on implantable sensors," *IEEE Sens. J.*, vol. 11, no. 12, pp. 3171–3182, Dec. 2011.

[6] A. Kim, M. Ochoa, R. Rahimi, and B. Ziaie, "New and emerging energy sources for implantable wireless microdevices," *IEEE Access*, vol. 3, pp. 89–98, 2015.

[7] K. Agarwal, R. Jegadeesan, Y. X. Guo, and N. V. Thakor, "Wireless power transfer strategies for implantable bioelectronics," *IEEE Rev. Biomed. Eng.*, vol. 10, pp. 136–161, Mar. 2017.

[8] D. Celinskis and B. C. Towe, "Wireless impedance measurements for monitoring peripheral vascular disease," in *Proc. 36th Annu. Int. Conf. IEEE Eng. Med. Biol. Soc.*, 2014, pp. 6937–6940.

[9] C. C. Collins, "Miniature passive pressure transensor for implanting in the eye," *IEEE Trans. Biomed. Eng.*, vol. BME-14, no. 2, pp. 74–83, Apr. 1967.

[10] M. F. Montero-Baker *et al.*, "The First-in-Man 'si Se Puede' Study for the use of micro-oxygen sensors (MOXYs) to determine dynamic relative oxygen indices in the feet of patients with limb-threatening ischemia during endovascular therapy," *J. Vascular Surgery*, vol. 61, no. 6, pp. 1501–1510.e1, 2015.

[11] O. G. M. S. Grimnes, *Bioimpedance and Bioelectricity Basics*, 3rd ed. New York, NY, USA: Academic, 2015.

[12] S. F. Cogan, "Neural stimulation and recording electrodes," *Annu. Rev. Biomed. Eng.*, vol. 10, pp. 275–309, 2008.

[13] E. S. A. M. Lepelaars, "Electromagnetic pulse distortion in living tissue," *Med. Biol. Eng. Comput.*, vol. 34, no. 3, pp. 213–220, 1996.

[14] M. Tudela-Pi, L. Becerra-Fajardo, A. Garcia-Moreno, J. Minguillon, and A. Ivorra, "Power transfer by volume conduction: In Vitro validated analytical models predict DC powers above 1 mW in injectable implants," *IEEE Access*, vol. 8, pp. 37808–37820, 2020.

[15] J. P. Reilly, "Excitation models," in *Applied Bioelectricity: From Electrical Stimulation to Electropathology*, J. P. Reilly, Ed. New York, NY, USA: Springer-Verlag, 1998, pp. 105–147.

[16] A. Vander Vorst, A. Rosen, and Y. Kotsuka, *RF/Microwave Interaction with Biological Tissues*. Hoboken, NJ, USA: Wiley, 2006.

[17] *IEEE Standard for Safety Levels With Respect to Human Exposure to Radio Frequency Electromagnetic Fields, 3 kHz to 300 GHz, I. I. C. on E. S.* IEEE SCC39. New York, NY, USA: The Institute of Electrical and Electronics Engineers, 2005.

[18] I. International Commission on Non-Ionizing Radiation Protection, "Guidelines for limiting exposure to time-varying electric, magnetic, and electromagnetic fields (up to 300 GHz)," *Health Phys.*, vol. 74, no. 4, pp. 494–522, 1998.

[19] D. Andreuccetti, R. Fossi, and C. Petrucci, "An Internet resource for the calculation of the dielectric properties of body tissues in the frequency range 10 Hz–100 GHz," *IFAC-CNR*, Florence, Italy, 1997. Based on data published by C. Gabriel *et al.* in 1996. [Online]. Available: http://niremf.ifac.cnr.it/tissprop/

[20] A. Mendez and J. Keys, "Density and composition of mammalian muscle," *Metabolism*, vol. 9, pp. 184–188, 1960.

[21] M. S. Wegmueller, M. Oberle, N. Felber, N. Kuster, and W. Fichtner, "Signal transmission by galvanic coupling through the human body," *IEEE Trans. Instrum. Meas.*, vol. 59, no. 4, pp. 963–969, Apr. 2010.

[22] L. Becerra-Fajardo, M. Tudela-Pi, and A. Ivorra, "Two-port networks to model galvanic coupling for intrabody communications and power transfer to implants," in *Proc. IEEE Biomed. Circuits Syst. Conf.*, 2018, pp. 1–4.

[23] M. S. Wegmueller *et al.*, "Galvanic coupling enabling wireless implant communications," *IEEE Trans. Instrum. Meas.*, vol. 58, no. 8, pp. 2618–2625, Aug. 2009.

[24] S. Grimnes and Ø. G. Martinsen, "Geometrical analysis," in *Bioimpedance and Bioelectricity Basics*, 2nd ed., Oxford, UK: Academic Press, 2008, pp. 161–204.

[25] E. Kreyszig, "Numeric linear algebra," in *Advanced Engineering Mathematics*, 9th ed., Hoboken, NJ, USA: Wiley, 2006, pp. 833–885.

[26] National Instruments NI-DAQ-6216, "USB-6216 Multifunction I/O Device," 2017.

[27] M. Tudela-Pi, L. Becerra-Fajardo, and A. Ivorra, "Powering implants by galvanic coupling: A validated analytical model predicts powers above 1 mW in injectable implants," *IFMBE Proc.*, vol. 68, no. 3, pp. 23–26, 2019.

[28] A. Ivorra, M. Shini, and B. Rubinsky, "Linear superposition electrical impedance tomography imaging with multiple electrical/biopsy probes," *IEEE Trans. Biomed. Eng.*, vol. 56, no. 5, pp. 1465–1472, May 2009.

[29] J. Riistama and J. Lekkala, "Electrochemical noise properties of different electrode materials in different electrolytes," in *Proc. 4th Int. Workshop Wearable Implantable Body Sensor Netw. IFMBE Proc.*, Berlin, Heidelberg, 2007, vol. 13, pp. 149–154.

[30] E. Huigen, A. Peper, and C. A. Grimbergen, "Investigation into the origin of the noise of surface electrodes," *Med. Biol. Eng. Comput.*, vol. 40, no. 3, pp. 332–338, 2002.

[31] R. E. Fromm, J. Varon, and L. R. Gibbs, "Congestive heart failure and pulmonary edema for the emergency physician," *J. Emerg. Med.*, vol. 13, no. 1, pp. 71–87, 1995.

[32] C. M. Yu *et al.*, "Intrathoracic impedance monitoring in patients with heart failure: Correlation with fluid status and feasibility of early warning preceding hospitalization," *Circulation*, vol. 112, no. 6, pp. 841–848, 2005.

[33] D. Catanzariti *et al.*, "Monitoring intrathoracic impedance with an implantable defibrillator reduces hospitalizations in patients with heart failure," *PACE - Pacing Clin. Electrophysiol.*, vol. 32, no. 3, pp. 363–370, 2009.

[34] L. Wang, "Fundamentals of Intrathoracic Impedance Monitoring in Heart Failure," *Amer. J. Cardiol.*, vol. 99, no. 10A, pp. 3–10, 2007.

[35] L. Wang *et al.*, "Feasibility of using an implantable system to measure thoracic congestion in an ambulatory chronic heart failure canine model," *PACE - Pacing Clin. Electrophysiol.*, vol. 28, no. 5, pp. 404–411, 2005.

[36] P. Horowitz and W. Hill, "JFET current source," in *The Art of Electronics*, New York, NY, USA : Cambridge Univ. Press, 2015, pp. 142–146.

[37] M. J. Kane, P. P. Breen, F. Quondamatteo, and G. Ólaighin, "BION microstimulators: A case study in the engineering of an electronic implantable medical device," *Med. Eng. Phys.*, vol. 33, no. 1, pp. 7–16, 2011.

[38] S. Salminger *et al.*, "Long-term implant of intramuscular sensors and nerve transfers for wireless control of robotic arms in above-elbow amputees," *Sci. Robot.*, vol. 4, no. 32, 2019, Art. no. eaaw6306.

[39] A. R. Mattson, J. D. Zhingre Sanchez, and P. A. Iaizzo, "The fixation tines of the Micra leadless pacemaker are atraumatic to the tricuspid valve," *PACE - Pacing Clin. Electrophysiol.*, vol. 41, no. 12, pp. 1606–1610, 2018.

[40] L. Becerra-Fajardo and A. Ivorra, "In vivo demonstration of addressable microstimulators powered by rectification of epidermically applied currents for miniaturized neuroprostheses," *PLoS One*, vol. 10, no. 7, pp. 1–19, 2015.

[41] L. Becerra-Fajardo, M. Schmidbauer, and A. Ivorra, "Demonstration of 2 mm thick microcontrolled injectable stimulators based on rectification of high frequency current bursts," *IEEE Trans. Neural Syst. Rehabil. Eng.*, vol. 25, no. 8, pp. 1343–1352, Aug. 2017.

[42] A. Ivorra, L. Becerra-Fajardo, and Q. Castellví, "In vivo demonstration of injectable microstimulators based on charge-balanced rectification of epidermically applied currents," *J. Neural Eng.*, vol. 12, no. 6, 2015, Art. no. 66010.

Shahid Malik received the master's degree from Jamia Millia Islamia University, New Delhi, India, with a specialization in control and instrumentation systems, in 2014. He is currently working toward the Ph.D. degree with the Indian Institute of Technology Bombay (IIT-Bombay), Mumbai, India. He was a Visiting Scholar with Tufts University Boston and UPF Barcelona during 2018–2019. His current research interests include instrumentation systems, analog circuit design, injectable biomedical implants, and flexible sensor system design.

Quim Castellví was born in Barcelona, Spain, in 1984. He received the B.Sc. degree in electronics engineering from the Universitat Politècnica de Catalunya, Terrassa, Spain, in 2009, the M.Sc. degree in biomedical engineering from the Universitat de Barcelona, Barcelona, Spain, in 2011, and the Ph.D. degree from the Universitat Pompeu Fabra, Barcelona, Spain, in 2017, with focus on scientific research in cancer treatment by means of electrical methods. He received a Competitive FPU Scholarship from the Spanish Ministry of Education to carry on the Ph.D. studies. The main research topic involves cancer treatment by means of electrical methods. In particular, he focuses on its scientific research in bioimpedance and electroporation.

Laura Becerra-Fajardo received the B.Sc. degree in electronic engineering from Universidad Nacional de Colombia, Bogot, Colombia, in 2008, the M.Sc. degrees in biomedical engineering from Universitat de Barcelona, Barcelona, Spain and Universitat Politècnica de Catalunya, Barcelona, Spain, in 2012, and the Ph.D. degree from Universitat Pompeu Fabra (UPF), Barcelona, Spain, in 2016. After working as a Research Engineer with the Translational Research and Knowledge Management team (R&D), Otto Bock GmbH, Duderstadt, Germany, she became a Postdoctoral Fellow with UPF. Her current research focuses mainly in exploring and designing miniaturized medical devices for sensing and electrical stimulation.

Marc Tudela-Pi was born in Vilanova de Bellpuig, Spain, in 1990. He received the M.Sc. degree in industrial electronic engineering from Universitat Politècnica de Catalunya, Barcelona, Spain, in 2013 and the M.Sc. degrees in biomedical engineering from Universitat de Barcelona, Barcelona, Spain, and Universitat Politècnica de Catalunya, Barcelona, Spain, in 2019. Since September 2017, he has been with the Biomedical Electronics Research Group, Pompeu Fabra University, Barcelona, Spain, where he is currently working toward the Ph.D. degree. He was a Control Engineer in the private sector designed high power electronic converters from 2013 to 2017. His current research interests include wireless power transfer for medical implants, bioelectronics, and bioimpedance.

Aracelys García-Moreno was born in Caracas, Venezuela, in 1982. She received the B.Sc. degree in electronic engineering from Universidad Simon Bolivar, Caracas, Venezuela, in 2005, and the M.Sc. degrees in biomedical engineering from Ghent University, Ghent, Belgium, and RWTH Aachen University, Aachen, Germany, in 2017. Since October 2017, she has been a Predoctoral Trainee Researcher and she is currently working toward the Ph.D. degree with the Department of Information and Communication Technologies, Universitat Pompeu Fabra, Barcelona, Spain. Her current research interests focus on the design, optimization and implementation of processes, techniques and components for the construction of implantable electronic devices for electrical stimulation.

Maryam Shojaei Baghini (Senior Member, IEEE) received the M.S. and Ph.D. degrees in electrical engineering from Sharif University of Technology, Tehran, Iran, in 1991 and 1999, respectively. She worked for more than two years in industry on the design of analog ICs. In 2001, she joined the Department of Electrical Engineering, IIT-Bombay, Mumbai, India, as a Postdoctoral Fellow, where she is currently a Professor. She has authored or co-authored more than 230 peer-reviewed international journal and conference papers. She is the inventor/co-inventor of six granted US patents, three granted Indian patents, and 43 more filed patent applications. Her research areas span from devices and sensors to the integrated instrumentation circuits and sensor systems, energy harvesting circuits and systems, and analog/mixed-signal/RF design for emerging applications. She has served as in the Technical Program Committee of several IEEE conferences, including recently as WSN Track Chair in IEEE Sensors Conference 2018 and 2019. She was a TPC Member of IEEE-ASSC from 2009 to 2014. She was the recipient/joint recipient of 12 awards, of which the recent award is the Best Paper Award in International Conference on VLSI Design 2019.

Antoni Ivorra received the Ph.D. degree in electronics engineering from the Universitat Politècnica de Catalunya, Barcelona, Spain, in 2005. He is currently an Associate Professor with Universitat Pompeu Fabra (UPF), Barcelona, Spain, where he leads the Biomedical Electronics Research Group. Prior to joining the UPF in 2010, he enjoyed a four-year postdoctoral stay with the University of California at Berkeley (2005–2009) followed by an eight-month Postdoctoral Position with the CNRS-Institut Gustave Roussy, Villejuif, France. During 1998–2005, he was with the Biomedical Applications Group, Centro Nacional de Microelectrónica, Bellaterra, Spain. He is the author or co-author of 50 publications in peer-reviewed journals, four book chapters, and more than 35 conference contributions. He is the inventor or co-inventor of 11 families of patent applications. His current research interests are focus on bioelectrical phenomena and, in particular, on exploring the use of these phenomena for implementing new methods and devices for biomedical applications. Specifically, his main research topics are electroporation, particularly for tissue ablation, electrical bioimpedance for diagnostic purposes and injectable electronics for neuroprosthetics.